

# Effect of Substrate Bias Voltage and Ti Doping on the Tribological Properties of DC Magnetron Sputtered $\text{MoS}_x$ Coatings

M. Akbarzadeh<sup>1</sup>, M. Zandrahimi<sup>\*1</sup> and E. Moradpour<sup>2</sup>

\*zandrahimi@mail.uk.ac.ir

Received: August 2018

Revised: September 2018

Accepted: October 2018

<sup>1</sup> Department of Metallurgy, Faculty of Engineering, Shahid Bahonar University of Kerman, Kerman, Iran.

<sup>2</sup> Department of Materials Engineering, Faculty of Engineering, Tarbiat Modares University, Tehran, Iran.

DOI: 10.22068/ijmse.16.2.10

**Abstract:** Molybdenum disulfide ( $\text{MoS}_2$ ) is one of the most widely used solid lubricants. In this work, composite  $\text{MoS}_x/\text{Ti}$  coatings were deposited by direct-current magnetron sputter ion plating onto plain carbon steel substrates. The  $\text{MoS}_x/\text{Ti}$  ratio in the coatings was controlled by sputtering the composite targets. The composition, microstructure, and mechanical properties of the coatings were explored using an energy dispersive analysis of X-ray (EDX), X-ray diffraction (XRD), nanoindentation and scratch techniques. The tribological behavior of the coatings was investigated using the pin-on-disc test at room temperature. With the increase of doped titanium content, the crystallization degree of the  $\text{MoS}_x/\text{Ti}$  composite coatings decreased. The  $\text{MoS}_x/\text{Ti}$  coatings showed a maximum hardness of 13 GPa at a dopant content of 5 at.% Ti and the  $\text{MoS}_x/\text{Ti}$  composite films outperformed the  $\text{MoS}_x$  films. Moreover, the films exhibited a steady state friction coefficient from 0.13 to 0.19 and the main wear mechanisms of the  $\text{MoS}_x/\text{Ti}$  coating in the air were abrasive, adhesive, and oxidation wear.

**Keywords:**  $\text{MoS}_x/\text{Ti}$  coating, Tribological properties, PVD, Low friction, Solid lubricant.

## 1. INTRODUCTION

Solid lubricants are materials that, despite being in the solid phase, are able to reduce the friction of surfaces. They overcome some inherent drawbacks to liquid lubrication and can be adopted in very harsh conditions (e.g., high temperature, heavy load, high vacuum, and strong oxidation). Under these conditions, liquid lubrication loses its lubricating function [1, 2].

Transition-metal dichalcogenides (TMDs;  $\text{MX}_2$  where M = Mo or W and X = S or Se) have been widely used in industry and research. The TMDs possess a layered structure with strong covalent bonding between the M and X atoms in a layer and weak Van der Waals forces between layers. Among  $\text{MX}_2$  coatings,  $\text{MoS}_2$  has been the most widely used as lubricant coating, but its tribological properties degrade in moist and high-temperature environments [3, 4].

$\text{MoS}_2$  has been applied to surfaces using a variety of methods, including hydrothermal synthesis [5, 6], physical vapor deposition [7], vertically aligned layers [4], photoluminescence

[8], chemical vapor deposition (CVD) [9], and chemical deposition [10]. Among these methods, PVD techniques have been most widely used in  $\text{MoS}_2$  coating deposition.

PVD magnetron sputtering, which is a very attractive deposition technique, involves applying high-energy plasma in a vacuum under the action of an electrical field to deposit the solid  $\text{MoS}_2$  on the substrate surface. Recent developments in magnetron sputtering technology have allowed the development of  $\text{MoS}_2$  composite coatings [11]. Several authors have explored adding metals and materials to improve the properties of  $\text{MoS}_2$  coating using the magnetron sputtering method. Some of metals studied include Au [12, 13], Zr [14, 15], Cu [16], Ag [17], Nb [18, 19], W [20], Ti [21, 22], Ta [12], Cr [21, 23], Al [24]. Also mixed metal or ceramic were studied such as  $\text{Mo}_2\text{N}$  [17],  $\text{TiAlN}$  [24],  $\text{TiN}$  [25, 26],  $\text{WS}_2$  [27, 28],  $\text{CrN}$  [29] or  $\text{Sb}_2\text{O}_3$  [30].

The addition of Ti to the  $\text{MoS}_2$  coating has drawn much attention due to the improvement of tribological performance in ambient air.  $\text{MoS}_2/\text{Ti}$  composite coatings are harder, more

adherent, significantly more wear resistant, and more load-bearing than pure MoS<sub>2</sub> coatings. They have similarly low friction to pure MoS<sub>2</sub> coatings and are less sensitive to atmospheric water vapor than pure MoS<sub>2</sub> coatings owing to the “gettering” effect of Ti during the wear process [31].

In the present work, MoS<sub>2</sub>/Ti coatings were deposited on plain carbon steel by direct-current (DC) magnetron sputtering ion plating. The properties of the coatings were evaluated and the effects of Ti inclusion in the MoS<sub>2</sub> coatings on their tribological performance in ambient air were investigated.

## 2. EXPERIMENTAL

Samples of plain carbon steel with a chemical composition of 0.15% C and 0.22% Si that measured 10 mm×5 mm×2 mm were used as substrates.

The substrates were cleaned ultrasonically in acetone and methanol for 15 mins and successively rinsed with deionized water and blown with dry air.

The MoS<sub>2</sub> coating were fabricated in DC magnetron sputtering ion plating equipment (model DST3 – S).

The vacuum system was pumped down to an ultimate base pressure of  $5 \times 10^{-4}$  Pa using a combination of diffusion and rotary pumps. Ar (99.95%) was used as the sputtering gas across the target surface. During the experiments, the substrate temperatures were between 19 and 25°C, as measured by thermometer; there was no external heating.

MoS<sub>2</sub> (purity 99.8%) and Ti (purity 99.99%) targets with 0, 5, 10, and 15 wt.% composite composition with a 50 mm diameter fixed on a magnetron were used. The composite targets were fabricated by ball milling the mixture of pure MoS<sub>2</sub> and Ti powders, followed by pressing the mixture under a pressure of 60 MPa in an Ar atmosphere at 850.

The microstructure and chemical composition of the surface and cross-section of the coatings were analyzed using a scanning electron microscopy (SEM) (Camscan MV2300) with energy dispersive spectroscopy (EDS). X-ray diffraction (XRD) was

utilized to identify the phases that formed in the surface layer of the coated sample, using Cu K $\alpha$  radiation ( $\lambda=1.5405 \text{ \AA}$ ).

The hardness and Young’s modulus were measured using the nanoindentation test (CSM) developed by Oliver and Pharr [32]. The maximum indentation depth, load, and max loading and unloading rate were 130 nm, 5000  $\mu\text{N}$ , and 60.00mN/min, respectively. Six indentations were applied on each coating and the average value was presented.

AHysitron Inc. TriboScope® nanomechanical test instrument with a two-dimensional transducer and commercial diamond cube corner indenter (three-sided pyramid geometry) with a tip radius of ~50–55 nm was used for the scratch tests. Three load-controlled ramping scratch tests were performed on each sample to determine the critical load of each coating.

Sliding wear tests were conducted using a pin-on-disc machine according to the ASTM G99-95. This equipment is controlled by its PC software, which allows the evolution of the friction coefficient to be observed. During the tests, the treated samples were rotating against a stationary AISI 52100 steel pin (with 4.576 mm hemispherical tip radius and hardness of 800 HV30) at a linear speed of 0.1 m/s under a load of 5 N.

## 3. RESULTS AND DISCUSSION

Among deposition parameters, a negative bias voltage applied to the substrates could significantly change film properties. A substrate bias voltage decreases the sulfur concentration and changes the stoichiometry of the coating, which deteriorates its lubricating properties. The stoichiometry of sputtered MoS<sub>2</sub> coatings can vary widely, from being sulfur-deficient to sulfur-rich (with sulfur/molybdenum ratios from 1.1 to 2.2). In addition, the bias voltage can clean the substrate by ion bombarding, which could enhance the adhesion [33]. Sputtered MoS<sub>2</sub> coatings were therefore deposited at different bias voltages to determine the optimal bias voltage.

The average growth rate of MoS<sub>2</sub> coatings with different bias voltages is shown in Fig. 1.

When the negative bias voltage was increased from -50 V to -100 V, the deposition rate of MoS<sub>2</sub> decreased sharply from 6.5 m/h to 1.5 m/h and then decreased slightly to 1 m/h with a further increase of the bias voltage to -150 V.

The MoS<sub>x</sub> films prepared by sputtering in our experiment did not form a stoichiometric MoS<sub>2</sub> composition. The S/Mo ratios–bias voltage relation obtained from the films deposited with bias voltages of 0, 50, 100, and 150 V is shown in Fig. 2. Since there is a natural tendency for sulfur to be lost during the MoS<sub>2</sub> deposition process, the general stoichiometry of the final coating was MoS<sub>x</sub> where generally  $x < 2$ . Due to the difference of the sputtering yield of Mo and S, the stoichiometry ratio ( $x$ ) varied between 1.2 and 1.8. The sputter yield is the number of atoms ejected from the target per incident ion. The reason for the decrease of the sulfur concentration is due to the preferential re-sputtering of S atoms with respect to Mo.

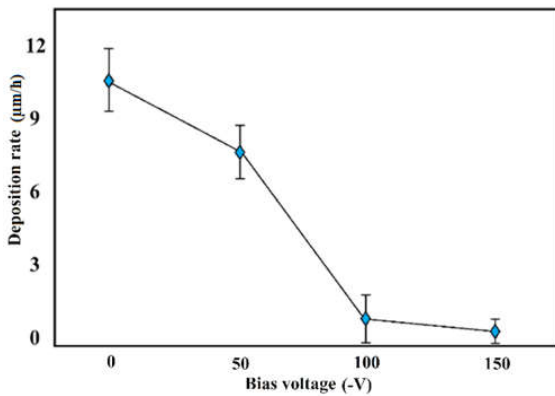


Fig. 1. Deposition rate versus the applied bias voltage.

Fig. 2 shows the effects of the substrate bias voltage on the S/Mo ratio and friction coefficient. As can be seen, the S/Mo ratio and friction coefficient decreased as the substrate bias voltage increased. Although it has not been established why sulfur defective structures ( $x < 2$ ) could have better friction properties than the perfect stoichiometric compound ( $x = 2$ ), this could be identified by a superior enhancement of the sulfur layer by strong bonding strength within the plane, without interaction with other layers [33].

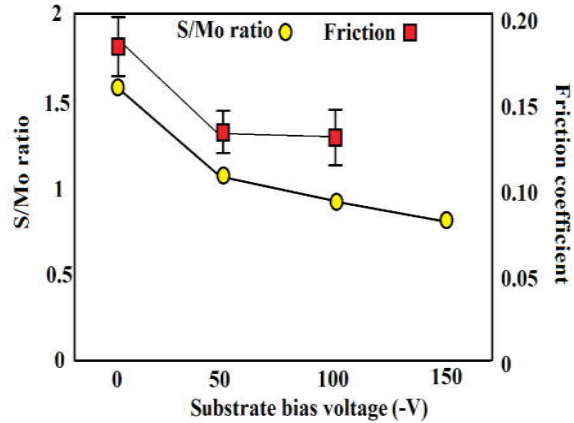


Fig. 2. Variation of the S/Mo ratio with a substrate bias voltage.

Representative plots of normal displacement and lateral force versus time from a ramping force nano-scratch test are shown in Fig. 3. These plots reveal distinct changes in curve profiles (circled) corresponding to film failure/delamination events that occurred during the ramping force nano-scratch test. The normal displacement and lateral force displayed in the data are explained as critical load ( $P_{crit}$ ) and critical depth ( $h_{crit}$ ), respectively.

3-D in-situ SPM image of MoS<sub>x</sub> coating at a voltage bias of -50 V after a 4000 µN ramping force nano-scratch test is shown in Fig. 4. Since the scratch groove depth is less than 1 µm the strength of adhesion is higher than coating cohesion.

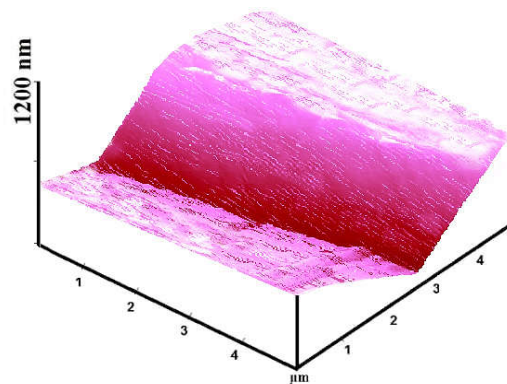


Fig. 3. 3-D in-situ SPM image of MoS<sub>x</sub> coating at a voltage bias of -50 V after a 4000 µN ramping force nano-scratch test.

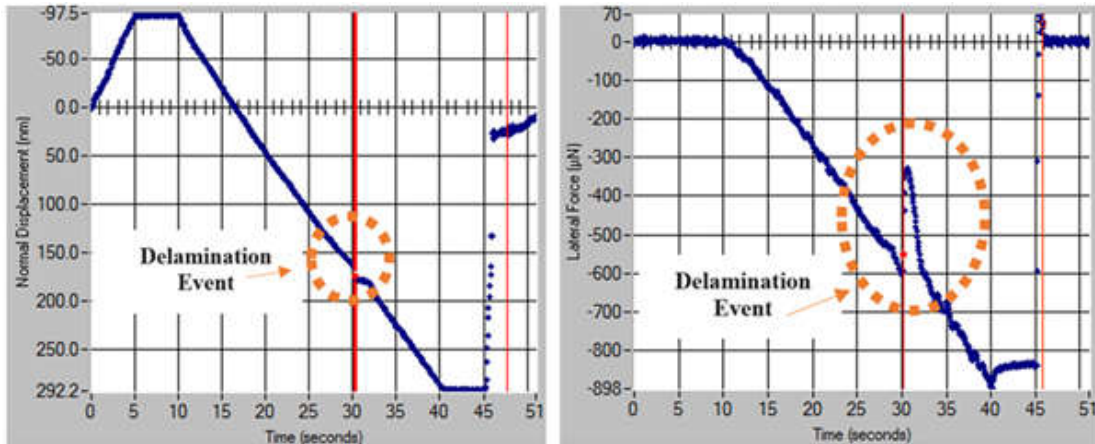


Fig. 4. Representative plots of lateral force and normal displacement versus time from a 4000  $\mu\text{N}$  ramping force nano-scratch test. The  $P_{\text{crit}}$  and  $h_{\text{crit}}$  are circled. (the applied bias voltage is -50 V)

Fig. 5 shows the variation of  $P_{\text{crit}}$  and  $h_{\text{crit}}$  data with a substrate bias voltage. The results clearly indicate that applying a voltage bias of -50 V improved the cohesive properties of coatings. The enhancement of adhesion with an increase in bias voltage can be attributed to the additional energy available to the growing film. High-energy atoms thus have greater mobility to find the low-energy sites on the surface to maximize the adhesion force. However, more increase in bias voltage would result in very high-energy bombardments that make the growing film being highly defective with a lower coating adhesion [34].

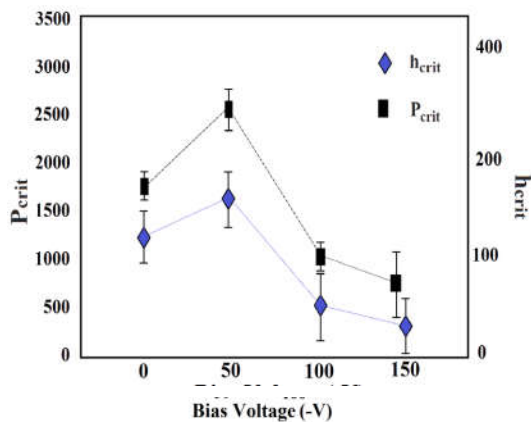
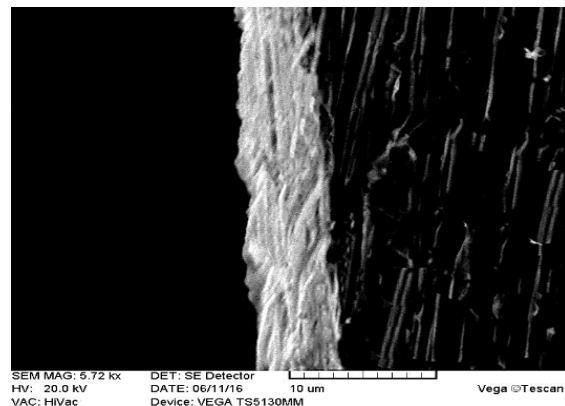


Fig. 5. Variation in  $P_{\text{crit}}$  and  $h_{\text{crit}}$  with a substrate bias voltage from 4 mN ramping force nano-scratch tests.

Fig. 6 shows a typical cross-sectional micrograph of sputtered  $\text{MoS}_2$  deposited at voltage bias of -50 V. The coating thickness is approximately 4  $\mu\text{m}$  and it shows good adherence to the substrate with no voids, pores, or discontinuities. The dense, compact, and coherent structure was attributed to the bias voltage of -50 V during coating deposition. The ion bombardment during deposition would play an important role in affecting the coatings morphology, composition, and mechanical properties. The energy dispersive analysis of X-ray (EDX) spectra of the coatings are shown in Fig. 6. No oxygen content was detected in the coatings. Since the coating thickness was less than 5  $\mu\text{m}$ , some peaks from the substrate can also be detected.

According to the better properties of  $\text{MoS}_x$  coatings which were deposited at a bias voltage of -50 V; the  $\text{MoS}_x/\text{Ti}$  composite coatings were also deposited at this bias voltage.



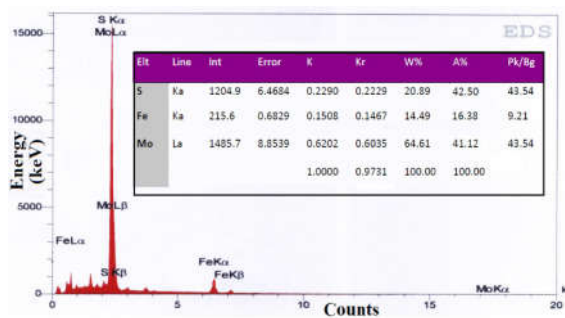


Fig. 6. SEM cross-section image of coating at a voltage bias of -50 V (a) and EDS spectrum (b).

The intensity of the  $\text{MoS}_2$  (100) diffraction peak was weakened and gradually disappeared with the increase of the doped Ti content. In addition to the diffraction peak that arose from the substrate, peaks were evident at approximately  $2\theta$  from  $29^\circ$ ,  $33^\circ$ , and  $44^\circ$  for the pure  $\text{MoS}_2$  coating.

Fig. 7 shows the XRD pattern of pure  $\text{MoS}_x$  coating. In addition to the diffraction peak that arose from the substrate, peaks were evident at approximately  $2\theta$  from  $14^\circ$ ,  $32^\circ$ ,  $33^\circ$ ,  $35^\circ$  and  $39^\circ$  for the pure  $\text{MoS}_2$  coating, which were assigned respectively to the  $\text{MoS}_2$  (002), (100), (101), (102), and (103) planes (according to JCPDS-ICDD card No 87-2416). Because there are very weak intensities of the peaks after  $60^\circ$  in the  $\text{MoS}_x$  coating XRD pattern, the XRD patterns are only reported between  $10^\circ$  and  $50^\circ$  in Fig. 8 for  $\text{MoS}_x/\text{Ti}$  coatings. The shape of the broad reflection in the  $10^\circ$  -  $50^\circ$  range is very similar to that found by Rigato et al. [20] and ascribed to random stacking of S-Mo-S sandwich layers in the structure.

Depending on the crystallographic orientation on the substrate surface,  $\text{MoS}_x$  coatings, in general, are classified into two orientation types: edge and basal. In the edge orientation (Fig. 9(a)), (002) was parallel to the substrate surface where the (100) and (110) planes of  $\text{MoS}_x$  crystallites were perpendicular to the substrate surface; in the basal orientation (Fig. 9(b)), the (100) edge plane of  $\text{MoS}_x$  crystallites was parallel to the substrate surface. The  $\text{MoS}_x$  coatings with the basal planes parallel to the sliding direction not only supply

good lubrication properties but are also more resistant to oxidation given that the edge sites are protected [33, 35].

The structure of the  $\text{MoS}_x/\text{Ti}$  composite coatings turned possibly into the dominated amorphous structure. The previous research by Filip et al. [36] showed that the sufficient addition of Ti prohibited the crystallization of  $\text{MoS}_2$  and promoted the formation of  $\text{Mo}_3\text{S}_4$ . There is no clear evidence in the XRD patterns for the existence of Ti sulfides or mixed Ti-Mo sulfides maybe due to the minimal content of these phases to be detected while no considerable scattered intensity of Mo and Ti oxides were detected.

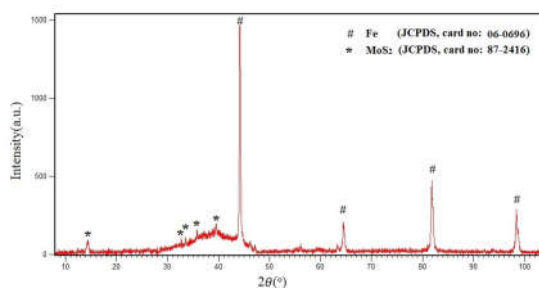


Fig. 7. XRD pattern of  $\text{MoS}_2$  coating.

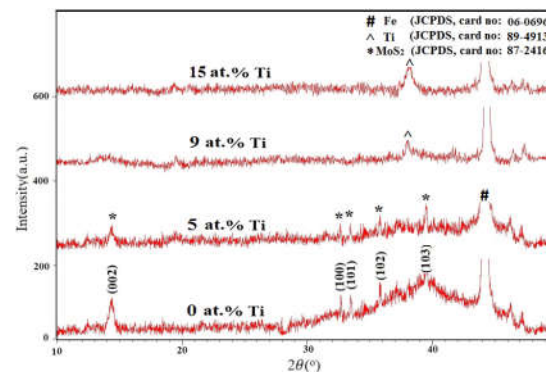


Fig. 8. XRD patterns of  $\text{MoS}_2$ -Ti composite coatings with different Ti content.

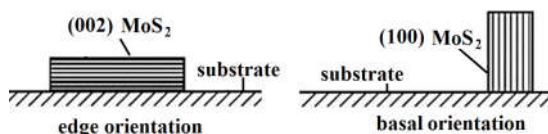


Fig. 9. Two categories of  $\text{MoS}_2$  coatings in terms of crystallographic orientations.

Fig. 10 shows the hardness and elastic modulus as a function of dopant concentration for MoS<sub>x</sub>/Ti coatings. It can be seen that the hardness of the films increased with the Ti content of the composite films. The high hardness of the MoS<sub>x</sub>/Ti coatings can be attributed to their dense structure. For the pure MoS<sub>x</sub> coating, the hardness was only approximately 7 GPa, while it increased to 14 GPa with the Ti content of 5 at.% (which was almost two times larger than that of pure MoS<sub>x</sub>). The hardness increased due to the structure densification with a certain saturation value of Ti content. Other researchers have reported that the hardness enhancement can be attributed to the solid solution hardening effect. Furthermore, when the metal doping content increased beyond the threshold value of 10 at.% Ti, the coating hardness decreased. This could be due to either the structure deterioration or the possible formation of discrete metallic particles [21, 37].

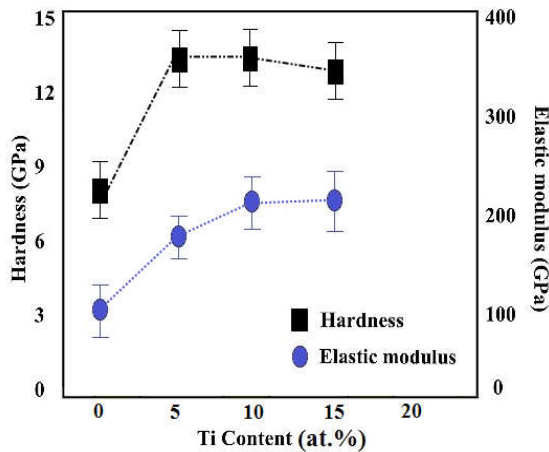


Fig. 10. The hardness and elastic modulus of the MoS<sub>x</sub>-Ti composite coatings as a function of Ti content (applied bias voltage is -50 V).

Critical load played a crucial role in the tribological property of the coatings. Fig. 11 shows the critical load of the MoS<sub>x</sub>/Ti composite coatings as a function of the Ti. Within the Ti content region of 0–5 at.%, increasing the Ti content led to the significant increase of the coatings' critical loads. It can thus be deduced that Ti concentration seemed to play a significant role in coating cohesion.

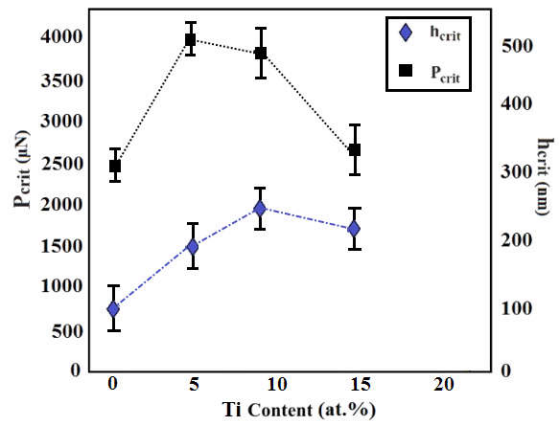


Fig. 11. Variation in critical load vs. weight fraction of Ti (applied bias voltage is -50 V).

In order to investigate the effect of doped Ti content on the tribological behavior of the MoS<sub>x</sub>/Ti composite coatings, pin-on-disc friction tests were performed under ambient air. Fig. 12 shows the variation of the friction coefficient for substrate, MoS<sub>x</sub> and MoS<sub>x</sub>/Ti (5 at.% Ti) as a function of wear cycles. As can be seen, doping Ti (5 at.%) into the MoS<sub>x</sub> coatings presented a relatively steady and low friction coefficient that was lower than of the pure MoS<sub>x</sub>. This indicates that the doped Ti improved the tribological properties of pure MoS<sub>2</sub> in the atmospheric environment.

In the initial stage, the friction coefficient kept in the relatively steady state and then rose sharply ( $\mu \sim 0.9$ : substrate friction coefficient) after 900 cycles for the MoS<sub>x</sub> coating (Fig. 12b) and 5500 cycles for the MoS<sub>x</sub>/Ti coating (Fig. 12c). The frictional 'noise' of the MoS<sub>x</sub>/Ti coating was much lower compared to the MoS<sub>x</sub> coating.

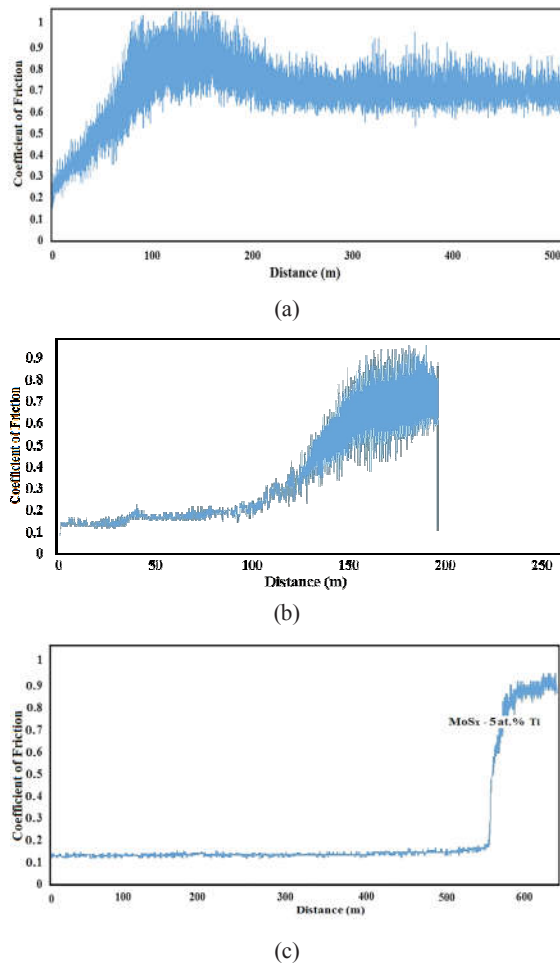


Fig. 12. Variation of the friction coefficient as a function of wear cycles for (a) substrate, (b) MoS<sub>x</sub> and (c) MoS<sub>x</sub>-5 at.% Ti film during the pin-on-disc wear test.

Fig. 13 shows the average friction coefficient of MoS<sub>x</sub>/Ti composite coatings with different Ti contents. As can be seen, with the increase of the Ti content, the average friction coefficient of the coating reduced from 0.20 (pure MoS<sub>x</sub>) to 0.14 (MoS<sub>x</sub>/Ti, 5 at.% Ti). According to the results of the pin-on-disc tests (as shown in Fig. 10), the addition of Ti to MoS<sub>x</sub>/Ti (<10 at.% Ti) increased the endurance of MoS<sub>x</sub> coatings. Although the MoS<sub>x</sub> coatings exhibited a low coefficient of friction ( $\mu \sim 0.2$ ), they failed after approximately 900 cycles during the pin-on-disc wear tests. The loss of endurance for MoS<sub>x</sub> is believed to be related to the reaction with oxygen and counter-face materials, which changed the wear mode of the coating and

no longer provided a lubrication effect.

During wear, MoS<sub>x</sub> could be oxidized into MoO<sub>3</sub>, which directly caused an abrasive effect as an anti-lubricating component, according to equation 1:



Owing to this chemical reaction, the nature of MoS<sub>x</sub> structure was affected significantly and consequently, the MoS<sub>x</sub> film lost its initial property with low shear strength. For this reason, a high coefficient of friction was observed in the air up to 1000 cycles [3].

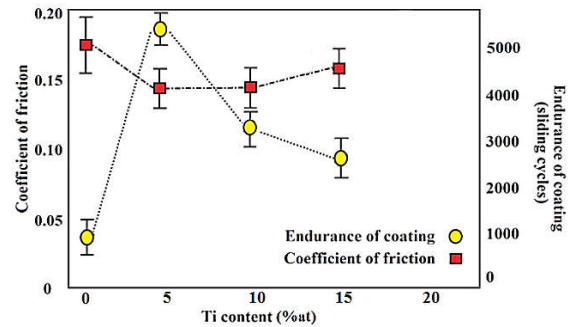


Fig. 13. Average friction coefficient of coating vs. weight fraction of Ti after 800 cycles and the endurance of coating under the load of 5 N and a sliding speed of 0.1 m/s in air.

Fig. 14 shows SEM micrographs and EDX spectra analysis of wear tracks for MoS<sub>x</sub> and MoS<sub>x</sub>/Ti. According to the EDX analysis, there were Ti, Mo and S on the worn surface of the MoS<sub>x</sub>/Ti coating after sliding cycles of 2000 while only Fe could be detected on the worn surface of MoS<sub>x</sub> after the same sliding cycles. The EDS analysis of the wear track regions of MoS<sub>2</sub> showed that the major element was Fe corresponding to severe wear.

Considering the low hardness and toughness, the MoS<sub>2</sub> coating was easily removed under the shear stress – which means that the production rate of detached material was high [38]. The reason that the MoS<sub>x</sub>/Ti coatings show better performance in a pin-on-disc test than MoS<sub>2</sub> has been studied by many researchers. Ding et al. proposed that the Ti atom move in the space between the sulfur planes and prevent the water

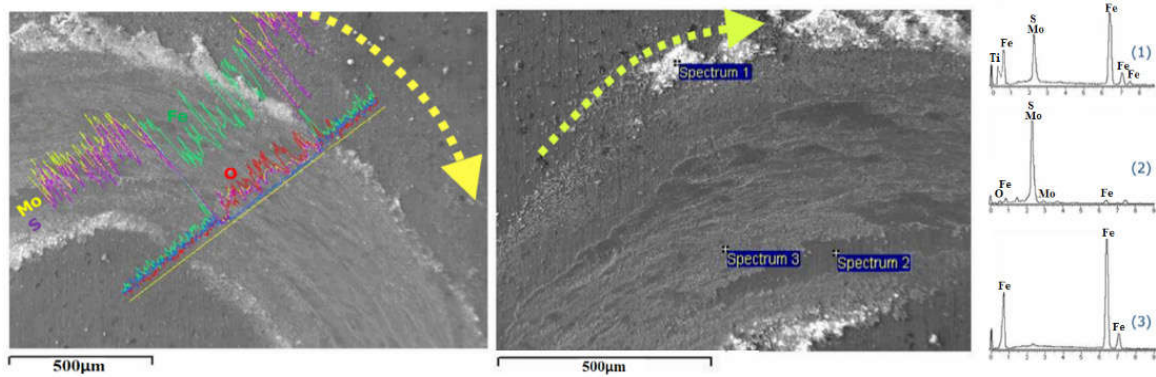


Fig. 14. SEM micrographs and EDX spectra analysis of wear tracks for (a) MoS<sub>2</sub> (b)

vapor from entering the coating [21]. Mikhailov et al. concluded that the role of metal is associated with structural modification of MoS<sub>x</sub> rather than the gettering of oxygen during wear test period [39]. During the wear tests conducted in this study, the oxygen easily substituted the sulfur deficient sites and formed the Mo-O-S structure, which caused the degradation of the tribological property. Ti contributed to the formation of stable MoS<sub>2</sub> and influenced the film's friction coefficient by preventing the gliding mechanism. The formation of a layer of TiO<sub>2</sub> could effectively prevent the oxidation of MoS<sub>x</sub> and thus improve the wear life of the coating [36, 37].

MoS<sub>x</sub>/Ti, after 2000 wear cycles (the yellow arrow indicates the sliding direction).

Fig. 15 shows the wear rates of MoS<sub>x</sub>/Ti coatings in various amounts of Ti. These wear rates decreased as Ti content increased. Due to the subsequent improvement in mechanical properties, the coating wear rate decreased in the region of 0–5 at.% Ti. The highest coating hardness and best adhesion together with the dense structure for the MoS<sub>2</sub>-5 wt.% Ti composite coating may, therefore, account for its best tribological behavior.

Fig.16 shows the SEM observations and roughness of the wear tracks of the MoS<sub>x</sub> coatings. These wear tracks had a rough, lumpy appearance and more debris was still collected at their edge. The wear track of the MoS<sub>x</sub> coating had ragged edges, which suggests that the coating delaminated by brittle rather than ductile fracture [40].

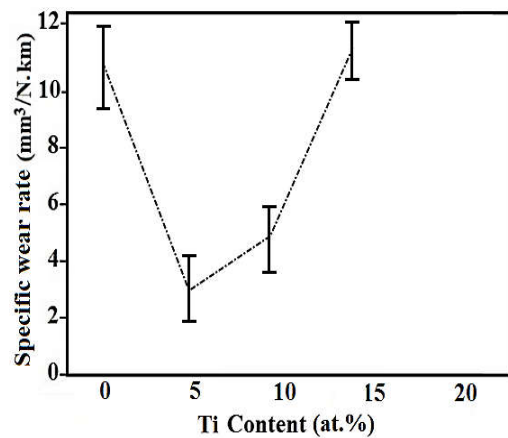


Fig. 15. Specific wear rates of MoS<sub>x</sub>/Ti coatings with different Ti content.

In order to determine dominant wear mechanisms, the wear tracks at the normal load of 5 N and after 800 wear cycles were examined by SEM and EDX, as shown in Fig. 17. Comparing wear tracks of samples with the same testing conditions revealed that the main wear mechanisms were different in each sample.

As can be seen in Fig. 16, many wide and deep grooves in the direction of slip were found. However, severe plastic deformations were present in MoS<sub>x</sub>/4 wt.% Ti coatings. The main wear mechanisms in the MoS<sub>x</sub> and MoS<sub>x</sub>/Ti coatings were therefore abrasive and adhesive, respectively.

Furthermore, the EDS analysis of the wear tracks showed that they had a high level of oxygen, which indicated tribo-chemical wear in the sample. The formation of oxides led to an



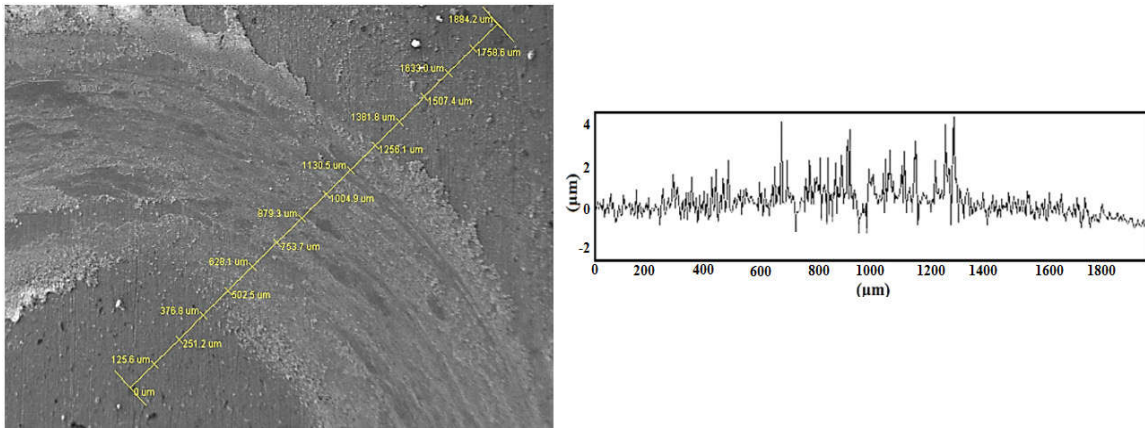


Fig. 16. SEM observations and the roughness of the MoS<sub>x</sub> worn surface.

increase of coefficient friction and a decrease in wear life. The presence of titanium atoms within the MoS<sub>2</sub> structure prevented the erosion of the water vapor and oxygen. With increasing Ti content, more MoS<sub>2</sub> was protected and less MoO<sub>3</sub> formation existed. The major wear mechanism in MoS<sub>x</sub> coatings is generally a mixture of abrasive and oxidation reaction.

#### 4. CONCLUSIONS

In this investigation, MoS<sub>x</sub>/Ti composite coatings with Ti contents varying from 0 to 13 wt.% were deposited onto steel substrate using a DC magnetron sputter ion plating process. The following conclusions can be drawn from the results:

1. Bias voltage has a significant effect on S/Mo in MoS<sub>2</sub> films so that it decreases as bias voltage increases. The highest NS/NMo (1.59) ratio was reached with the lowest bias (0 V).
2. With the decrease of doped titanium content, the phase crystallinity of the MoS<sub>2</sub>-Ti composite coatings was increased.
3. The MoS<sub>x</sub>/Ti coatings that were deposited by means of magnetron sputtering showed excellent tribological properties.
4. Within the Ti content region of 0–5 wt.%, increasing the Ti content led to a significant increase in the coating's critical load.
5. The MoS<sub>x</sub>/Ti coatings exhibited a steady state friction coefficient ranging from 0.13 to 0.19.
6. Adding Ti to MoS<sub>x</sub> coatings improved their adhesion to the steel substrate and hardness as well as increased the wear performance of MoS<sub>x</sub> coatings under atmospheric conditions.
7. Adding Ti to MoS<sub>x</sub> can significantly avoid humidity or tribo-chemical effects on the MoS<sub>2</sub> layer and hence significantly increase the wear life.
8. MoS<sub>x</sub>/Ti coatings showed superior wear

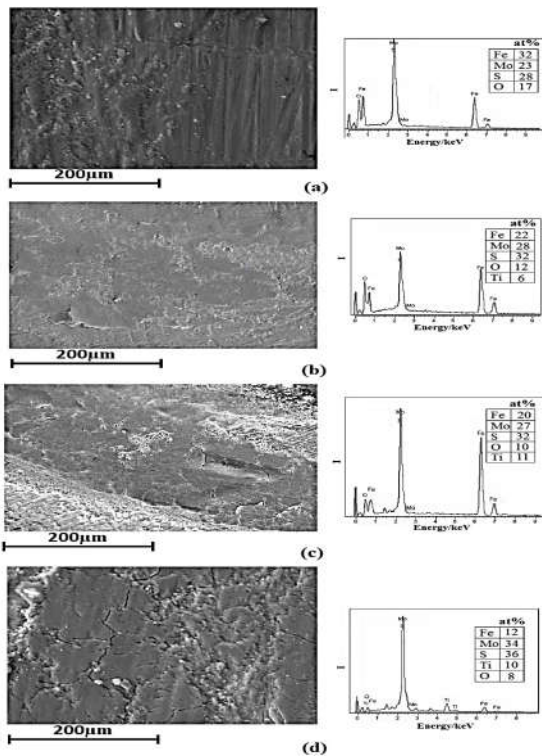


Fig. 17. Worn morphologies and EDX analysis of the synthetic MoS<sub>x</sub>/Ti coatings with different Ti content (a) pure MoS<sub>x</sub> (b) 5at.% Ti, after 800 wear cycles.

- resistance over  $\text{MoS}_x$  coating.
9. The major wear mechanism in  $\text{MoS}_x$  coatings was a mixture of abrasive and oxidation reactions.
  10. The main wear mechanisms of  $\text{MoS}_x/\text{Ti}$  coatings were adhesive in air.

## REFERENCES

1. Miyoshi, K., "Solid Lubrication Fundamentals and Applications: CRC Press.", 2001.
2. Wang, H., Xu, B. and Liu, J., "Micro and Nano Sulfide Solid Lubrication: Springer Berlin Heidelberg.", 2013.
3. Kim, S. S., Ahn, C., W. and Kim, T. H., "Tribological characteristics of magnetron sputtered  $\text{MoS}_2$  films in various atmospheric conditions.", *KSME international journal*. 2002, 16, 1065-1071.
4. Kong, D., Wang, H., Cha, J. J., Pasta, M., Koski, K. J. and Yao, J., "Synthesis of  $\text{MoS}_2$  and  $\text{MoSe}_2$  films with vertically aligned layers.", *Nano letters*. 2013, 13, 1341-1347.
5. Peng, Y., Meng, Z., Zhong, C., Lu, J., Yu, W. and Jia, Y., "Hydrothermal Synthesis and Characterization of Single-Molecular-Layer  $\text{MoS}_2$  and  $\text{MoSe}_2$ .", *Chemistry Letters*. 2001, 8, 772-773.
6. Luo, H., Xu, C., Zou, D., Wang, L. and Ying, T., "Hydrothermal synthesis of hollow  $\text{MoS}_2$  microspheres in ionic liquids/water binary emulsions.", *Materials letters*. 2008, 62, 3558-3560.
7. Gong, C., Huang, C., Miller, J., Cheng, L., Hao, Y. and Cobden, D., "Metal contacts on physical vapor deposited monolayer  $\text{MoS}_2$ .", *ACS nano*. 2013, 7, 11350-1137.
8. Ji, Q., Zhang, Y., Gao, T., Zhang, Y., Ma, D. and Liu, M., "Epitaxial monolayer  $\text{MoS}_2$  on mica with novel photoluminescence.", *Nano letters*. 2013, 13, 3870-3877.
9. Lee, Y., H., Zhang, X., Q., Zhang, W., Chang, M. T., Lin C. T. and Chang K. D., "Synthesis of Large-Area  $\text{MoS}_2$  Atomic Layers with Chemical Vapor Deposition.", *Advanced Materials*. 2012, 24, 2320-2325.
10. Pramanik, P. and Bhattacharya, S., "Deposition of molybdenum chalcogenide thin films by the chemical deposition technique and the effect of bath parameters on these thin films.", *Materials research bulletin*. 1990, 25, 15-23.
11. Onate, J., Brizuela, M., Viviente, J., Garcia, A., Braceras, I. and Gonzalez, D., " $\text{MoS}_x$  lubricant coatings produced by PVD technologies.", *Transactions of the IMF*. 2013, 85, 75-81.
12. Yin, Z., Chen, B., Bosman, M., Cao, X., Chen, J. and Zheng, B., "Au Nanoparticle- Modified  $\text{MoS}_2$  Nanosheet-Based Photoelectrochemical Cells for Water Splitting. *Small*.", 2014, 10, 3537-3543.
13. Scharf, T., Goeke, R., Kotula, P. and Prasad, S., "Synthesis of Au- $\text{MoS}_2$  Nanocomposites: Thermal and Friction-Induced Changes to the Structure.", *ACS applied materials and interfaces*. 2013, 5, 11762-11767.
14. Jianxin, D., Wenlong, S., Hui, Z. and Jinlong, Z., "Performance of PVD  $\text{MoS}_2/\text{Zr}$ -coated carbide in cutting processes. *International Journal of Machine Tools and Manufacture*.", 2008, 48, 1546-1552.
15. Wenlong, S., Jianxin, D., Hui, Z. and Pei, Y., "Study on cutting forces and experiment of  $\text{MoS}_2/\text{Zr}$  coated cemented carbide tool.", *The International Journal of Advanced Manufacturing Technology*. 2010, 49, 903-909.
16. Zhang, Y., Shockley, J. M., Vo, P. and Chromik, R. R., "Tribological Behavior of a Cold-Sprayed Cu- $\text{MoS}_2$  Composite Coating During Dry Sliding Wear.", *Tribology Letters*. 2016, 62, 1-12.
17. Aouadi, S. M., Paudel, Y., Luster, B., Stadler, S., Kohli, P. and Muratore, C., "Adaptive  $\text{Mo}_2\text{N}/\text{MoS}_2/\text{Ag}$  tribological nanocomposite coatings for aerospace applications.", *Tribology Letters*. 2008, 29, 95-103.
18. Arslan, E., Totik, Y., Bayrak, O., Efeoglu, I. and Celik, A., "High temperature friction and wear behavior of  $\text{MoS}_2/\text{Nb}$  coating in ambient air.", *Journal of coatings technology and research*. 2010, 7, 131-137.
19. Bhushan B., "Introduction to Tribology.", Wiley, 2013.
20. Rigato, V., Maggioni, G., Patelli, A., Boscarino, D., Renevier, N. M. and Teer, D. G., "Properties of sputter-deposited  $\text{MoS}_2$ /metal composite coatings deposited by closed field unbalanced magnetron sputter ion plating.", *Surface and Coatings Technology*. 2000, 131, 206-210.
21. Ding, X., Zeng, X., He, X. and Chen, Z., "Tribological properties of Cr- and Ti-doped  $\text{MoS}_2$  composite coatings under different humidity atmosphere.", *Surface and Coatings Technology*. 2010, 205, 224-231.
22. Hui, Z., Jun, Z., Qing ping, W., Zhi-hua, W. and Rui-peng, S., "The effect of Ti content on the structural and mechanical properties of  $\text{MoS}_2$ -Ti composite coatings deposited by unbalanced magnetron sputtering system.", *Target*. 2011, 5, 0-5.
23. Kao, W., "Tribological properties and high speed drilling application of  $\text{MoS}_2$ -Cr coatings.", *Wear*. 2005, 258, 812-825.
24. Yongliang, L. and Sunkyu, K., "Microstructural and tribological behavior of  $\text{TiAlN}/\text{MoS}_2$ -Ti coat-

- ings.”, *Rare Metals*. 2006, 25, 326-330.
25. Xu, G., Zhou, Z. and Liu, J., “A comparative study on fretting wear-resistant properties of ion-plated TiN and magnetron-sputtered MoS<sub>2</sub> coatings.”, *Wear*. 1999, 224, 211-215.
  26. Gangopadhyay, S., Acharya, R., Chattopadhyay, A. and Paul, S., “Composition and structure–property relationship of low friction, wear resistant TiN–MoS<sub>x</sub> composite coating deposited by pulsed closed-field unbalanced magnetron sputtering.”, *Surface and Coatings Technology*. 2009, 203, 1565-1572.
  27. Watanabe, S., Noshiro, J. and Miyake, S., “Friction properties of WS<sub>2</sub>/MoS<sub>2</sub> multilayer films under vacuum environment.”, *Surface and Coatings Technology*. 2004, 188, 644-648.
  28. Noshiro, J., Watanabe, S. and Miyake, S., “Deposition and tribological properties of WS<sub>2</sub>/MoS<sub>2</sub>/C solid lubricating multilayer films. Japanese journal of tribology.”, 2004, 49, 621-630.
  29. Carrera, S., Salas, O., Moore, J. and Woolverton, A., “Sutter E. Performance of CrN/MoS<sub>2</sub> (Ti) coatings for high wear low friction applications.”, *Surface and Coatings Technology*. 2003, 167, 25-32.
  30. Zabinski, J., Bultman, J., Sanders, J. and Hu, J., “Multi-environmental lubrication performance and lubrication mechanism of MoS<sub>2</sub>/Sb<sub>2</sub>O<sub>3</sub>/C composite films.”, *Tribology Letters*. 2006, 23, 155-163.
  31. Renevier, N. M., Fox, V. C., Teer, D. G. and Hampshire, J., “Coating characteristics and tribological properties of sputter-deposited MoS<sub>2</sub>/metal composite coatings deposited by closed field unbalanced magnetron sputter ion plating.”, *Surface and Coatings Technology*. 2000, 127, 24-37.
  32. Pharr, G., Oliver, W., “Measurement of thin film mechanical properties using nanoindentation.”, *Mrs Bulletin*. 1992, 17, 28-33.
  33. Yang, J., F., Parakash, B., Hardell, J. and Fang, Q. F., “Tribological properties of transition metal di-chalcogenide based lubricant coatings.”, *Frontiers of Materials Science*. 2012, 6, 116-127.
  34. Gangopadhyay, S., Acharya, R., Chattopadhyay, A. and Paul, S., “Effect of substrate bias voltage on structural and mechanical properties of pulsed DC magnetron sputtered TiN–MoS<sub>x</sub> composite coatings.”, *Vacuum*. 2010, 84, 843-850.
  35. Seitzman, L., Bolster, R., Singer, I. and Wegand, J., “Relationship of endurance to microstructure of IBAD MoS<sub>2</sub> coatings. *Tribology transactions*.”, 1995, 38, 445-451.
  36. Ilie FI, Tita C. Tribological properties of solid lubricant nanocomposite coatings obtained by magnetron sputtered of MoS<sub>2</sub>/metal (Ti, Mo) nanoparticles. *Proc. Rom. Acad. Ser. A Math. Phys. Tech. Sci. Inf. Sci.* 2007, 1, 1-5.
  37. Qin, X., Ke, P., Wang, A. and Kim, K. H., “Microstructure, mechanical and tribological behaviors of MoS<sub>2</sub>-Ti composite coatings deposited by a hybrid HIPIMS method.”, *Surface and Coatings Technology*. 2013, 228, 275-281.
  38. Zhu, X., Lauwerens, W., Cosemans, P., Van Stapen, M., Celis, J. P. and Stals, L., “Different tribological behavior of MoS<sub>2</sub> coatings under fretting and pin-on-disk conditions.”, *Surface and Coatings Technology*. 2003, 163, 422-428.
  39. Mikhailov, S., Savan, A., Pflüger, E., Knoblauch, L., Hauert, R. and Simmonds, M., “Morphology and tribological properties of metal (oxide)–MoS<sub>2</sub> nanostructured multilayer coatings.”, *Surface and Coatings Technology*. 1998, 105, 175-183.
  40. Singer, I., Fayeulle, S. and Ehni, P., “Wear behavior of triode-sputtered MoS<sub>2</sub> coatings in dry sliding contact with steel and ceramics.”, *Wear*. 1996, 195, 7-20.